

Electron-phonon coupling and two-band superconductivity of Al- and C-doped MgB₂

O. De la Peña-Seaman,^{1,2} R. de Coss,¹ R. Heid,² and K.-P. Bohnen²

¹*Departamento de Física Aplicada, Centro de Investigación y de Estudios Avanzados del IPN
Apartado Postal 73 Cordemex 97310 Mérida, Yucatán, México*

²*Karlsruher Institut für Technologie (KIT), Institut für Festkörperphysik
P.O. Box 3640, D-76021 Karlsruhe, Germany*

(Dated: December 10, 2010)

Abstract

We have studied the electron-phonon and superconducting properties of the Mg_{1-x}Al_xB₂ and MgB₂(1-y)C_{2y} alloys within the framework of density functional theory using the self-consistent virtual-crystal approximation. For both alloys, the Eliashberg spectral functions and the electron-phonon coupling constants have been calculated in the two-band model for several concentrations up to $x(\text{Al}) = 0.55$ and $y(\text{C}) = 0.175$. We solved numerically the two-band Eliashberg gap equations without considering interband scattering. Using a single parameter for the Coulomb pseudopotential, which was determined for the undoped compound, we were able to reproduce the experimental doping dependence of Δ_σ , Δ_π , and T_c for both alloys on a quantitative level. In particular, the observed differences in the doping range of superconductivity between Al and C doping indicate a pronounced influence of the doping site, which can be explained naturally in the present approach without the need to invoke interband scattering, suggesting that this factor plays only a minor role.

PACS numbers: 74.70.Ad, 74.62.Dh, 63.20.kd, 71.15.Mb

I. INTRODUCTION

The discovery of superconductivity in 2001 in the intermetallic compound MgB_2 , with a critical temperature $T_c \approx 39 \text{ K}$ ¹, has motivated a lot of theoretical and experimental studies in order to understand the origin and characteristics of the relatively high T_c in this material. It is now generally accepted that MgB_2 is a phonon-mediated superconductor, and that the high transition temperature arises due to a combination of several peculiar features in its electronic structure and electron-phonon coupling, which conspire to produce a superconducting state with multiple gaps²⁻¹⁰. Its electronic band structure in the vicinity of the Fermi energy consists of two bonding σ bands corresponding to in-plane $s - p_x - p_y$ (sp^2) hybridization in the boron layer and two π bands (bonding and anti-bonding) formed by hybridized boron p_z orbitals. A substantial part of the electron-phonon coupling has its origin in the interaction of states at the σ -band Fermi surfaces with one specific phonon mode, the B-B bond stretching mode with E_{2g} symmetry at the Γ point^{4,6,11-14}. In addition, MgB_2 possesses two distinct superconducting gaps associated with the σ and π Fermi surfaces. This superconducting state can be described within a multiband version of the Eliashberg theory where the pairing interaction is split into intra- and interband contributions^{11,15-17}.

In the search for related compounds with similar outstanding superconducting properties, only a few variants of MgB_2 have been found. Among them, two alloy systems could be successfully synthesized based on the partial substitution of Mg by Al¹⁸⁻²¹ and B by C²²⁻²⁶, respectively. Both substitutions provide electron doping to the alloy and lead to a reduction of T_c . For $\text{Mg}_{1-x}\text{Al}_x\text{B}_2$ and $\text{MgB}_{2(1-y)}\text{C}_{2y}$, loss of superconductivity is found for $x > 0.5$ ¹⁸⁻²¹ and $y > 0.15$ ²²⁻²⁶, respectively. A correlation between the T_c reduction and the filling of the hole-type σ -bands as a function of Al-doped content was found by *first principles* calculations within the virtual-crystal approximation^{27,28}. In parallel with the reduction of T_c also a decrease of the superconducting gaps Δ_σ and Δ_π has been observed. For single crystals as well as polycrystals Al doping was found to decrease both σ and π gaps monotonically, which, however, stay distinguishable even for T_c as low as 10 K ($x \approx 0.32$)²⁹⁻³⁵. These observations indicate that the interband scattering $\Gamma_{\sigma\pi}$ remains small even at high doping levels, and is insufficient to produce a merging of the σ and π gaps. On contrast, for the C-doped system, contradictory experimental results have been reported with respect to the question

if the superconducting gaps merge as a function of doping^{31,33,36–38}. In all experiments a decrease of both gaps with C doping was observed. There are point-contact tunneling^{36,37}, point-contact spectroscopy³³ and photoemission spectroscopy³⁸ measurements that show a clear difference between the σ and π gaps at all doping levels. However, there exists also point-contact spectroscopy measurements³¹ that suggest a merging of the gaps at $T_c \approx 17$ K ($y \approx 0.13$). This was then interpreted as a doping-induced increase of the interband scattering $\Gamma_{\sigma\pi}$, which tends to reduce gap anisotropies.

From the theoretical point of view, many investigations have been performed to study the doping dependence of the structural^{27,39}, electronic^{27,40–44}, vibrational^{44–47} and superconducting properties^{41,44,46,48–53} of the $\text{Mg}_{1-x}\text{Al}_x\text{B}_2$ and $\text{MgB}_2(1-y)\text{C}_{2y}$ systems using different approximations for the simulation of the alloys, like the supercell approach^{39,40,45,47,49}, the rigid band approximation (RBA)⁴⁴, the virtual-crystal approximation (VCA)^{3,27,43,46}, the coherent potential approximation (CPA)^{41,42,48}, and the Korringa-Kohn-Rostoker coherent potential approximation (KKR-CPA)⁵³. However, in particular for the supercell and CPA approaches, the studies have been limited to a few Al or C concentrations only, because these calculations are computationally very demanding, especially if one is interested in very low (close to Mg or B) or high (close to Al) concentrations. Additionally, in these approaches the symmetry of the original system is lost, which complicates the interpretation and understanding of experimental results as a function of doping.

In this paper, we present a study of the electron-phonon and superconducting properties of $\text{Mg}_{1-x}\text{Al}_x\text{B}_2$ and $\text{MgB}_2(1-y)\text{C}_{2y}$ within the framework of density functional theory⁵⁴ using the self-consistent virtual-crystal approximation (VCA)^{27,55–57}. We calculate the electron-phonon (e-ph) properties such as the Eliashberg function, $\alpha_{ij}^2 F(\omega)$, and the e-ph coupling constant, λ_{ij} , within the two-band model as a function of doping. By solving the two-band Eliashberg gap equations on the imaginary axis we obtain the superconducting gaps, Δ_σ and Δ_π , and the value of T_c as a function of x or y for the $\text{Mg}_{1-x}\text{Al}_x\text{B}_2$ and $\text{MgB}_2(1-y)\text{C}_{2y}$ alloys, respectively. The evolution of these quantities is analyzed and discussed in connection with changes in the electronic and vibrational properties.

II. COMPUTATIONAL DETAILS

The calculations were performed with the mixed-basis pseudopotential method (MBPP)^{58,59}. For Mg/Al and B/C norm-conserving pseudopotentials were constructed according to the Vanderbilt description⁶⁰. Details of pseudopotentials, basis functions and calculational aspects for ground-state and phonon properties can be found in a previous publication²⁸. The $\text{Mg}_{1-x}\text{Al}_x\text{B}_2$ and $\text{MgB}_{2(1-y)}\text{C}_{2y}$ alloys were modeled in the self-consistent virtual-crystal approximation (VCA)^{27,28,55–57,61–63}. The VCA is implemented within the MBPP method^{58,59} by generating new pseudopotentials with a fractional nuclear charge at the Mg or B site for each x and y , respectively (Al: $Z=12+x$ and C: $Z=5+y$), and by adjusting the valence charge accordingly²⁸. From our previous results for the electronic and vibrational properties²⁸ the screened electron-phonon matrix elements were calculated via density functional perturbation theory^{54,64–66}, which are the key elements of the Eliashberg theory^{67–70}. The calculations employ the PBE version of the generalized gradient approximation (GGA)^{71–73}, and are performed at the optimal lattice parameters for each doping level²⁸. Eliashberg functions for all band combinations were obtained by standard Fourier interpolation of quantities calculated with a dense $36 \times 36 \times 36$ k -point mesh and a $6 \times 6 \times 6$ q -point mesh. The original four-band Eliashberg functions are projected onto an effective two-band model by averaging over the two σ and the two π bands, respectively. The partial and total Eliashberg functions are given by the following expressions,

$$\alpha_{ij}^2 F(\omega) = \frac{1}{N_i} \sum_{\mathbf{q}\nu} \delta(\omega - \omega_{\mathbf{q}\nu}) \sum_{\mathbf{k}, \mathbf{k}_n} |g_{\mathbf{k},i,\mathbf{k}_n,j}^{\mathbf{q}\nu}|^2 \delta(\epsilon_{\mathbf{k},i} - \epsilon_F) \delta(\epsilon_{\mathbf{k}_n,j} - \epsilon_F), \quad (1)$$

$$\alpha^2 F(\omega) = \frac{1}{N_{tot}} \sum_{ij} N_i \alpha_{ij}^2 F(\omega), \quad (2)$$

where i and j are the band indices σ or π , N_i (N_{tot}) is the partial (total) electronic density of states at the Fermi level (per atom and spin), and $g_{\mathbf{k},i,\mathbf{k}_n,j}^{\mathbf{q}\nu}$ is the e-ph matrix element for scattering of an electron from a Bloch state with momentum \mathbf{k} to another Bloch state $\mathbf{k}_n = \mathbf{k} + \mathbf{q}$ by a phonon $\mathbf{q}\nu$ (ν indicates the branch index and $\omega_{\mathbf{q}\nu}$ is the phonon frequency).

In a similar way, the partial and total e-ph coupling parameters (λ) are expressed as follows,

$$\lambda_{ij} = 2 \int \frac{d\omega}{\omega} \alpha_{ij}^2 F(\omega), \quad (3)$$

$$\lambda_{tot} = \frac{1}{N_{tot}} \sum_{ij} N_i \lambda_{ij}, \quad (4)$$

Within the two-band model, there are three independent contributions to $\alpha_{ij}^2 F(\omega)$: two intraband ($\pi\pi$ and $\sigma\sigma$) and one interband $\alpha_{\pi\sigma}^2 F(\omega) = \frac{N_\sigma}{N_\pi} \alpha_{\sigma\pi}^2 F(\omega)$. With the knowledge of $\alpha_{ij}^2 F(\omega)$, the two-band Eliashberg gap equations^{67–69,74} on the imaginary axis were numerically solved in order to obtain the gap values and T_c for each given Al or C concentration, respectively. This procedure has been previously used in similar studies of undoped MgB₂^{16,50}. The solution involves four non-linear coupled equations for the Matsubara gaps $\Delta_i(i\omega_n)$ and the renormalization functions $Z_i(i\omega_n)$,

$$\Delta_i(i\omega_n) Z_i(i\omega_n) = \pi T \sum_{m,j} [\Lambda_{ij}(i\omega_m - i\omega_n) - \mu_{ij}^*(\omega_c) \theta(\omega_c - |\omega_m|)] N_{\Delta 1}^j(i\omega_m), \quad (5)$$

$$Z_i(i\omega_n) = 1 + \frac{\pi T}{\omega_n} \sum_{m,j} \Lambda_{ij}(i\omega_m - i\omega_n) N_{\Delta 0}^j(i\omega_m), \quad (6)$$

where θ is the Heaviside function, and μ_{ij}^* is the Coulomb pseudopotential, ω_c a cutoff frequency (chosen as $\omega_c \approx 10\omega_{ph}^{max}$) and $\omega_n = \pi T(2n - 1)$, with $n = 0, \pm 1, \pm 2, \dots$, is the discrete set of Matsubara frequencies. The pairing interaction is contained in the kernel

$$\Lambda_{ij}(i\omega_m - i\omega_n) = 2 \int_0^\infty \frac{\omega \alpha_{ij}^2 F(\omega) d\omega}{\omega^2 + (\omega_n - \omega_m)^2}, \quad (7)$$

and we defined the following quantities:

$$N_{\Delta 1}^j(i\omega_m) = \frac{\Delta_j(i\omega_m)}{\sqrt{\omega_m^2 + \Delta_j^2(i\omega_m)}}, \quad (8)$$

$$N_{\Delta 0}^j(i\omega_m) = \frac{\omega_m}{\sqrt{\omega_m^2 + \Delta_j^2(i\omega_m)}}. \quad (9)$$

In order to keep the number of adjustable parameter to a minimum, we approximated the Coulomb pseudopotential matrix μ_{ij}^* , which is a two-by-two matrix in the case of the two-band model, by a diagonal form proposed earlier⁷⁵ as $\mu_{ij}^* = \mu_0^* \delta_{ij}$.⁷⁶ The gap values were identified with $\Delta_i(i\omega_1)$, which corresponds to the point on the imaginary axis which is

closest to the real axis. Test calculations solving the Eliashberg equations on the real axis indicated that this approximation is accurate on the level of 1% or better.

III. RESULTS AND DISCUSSION

Based on our previous results for the electronic and vibrational properties²⁸, we have calculated the electron-phonon coupling quantities of the two-band model ($\alpha_{ij}^2 F(\omega)$ and λ_{ij} with $i, j = \sigma, \pi$) for the ranges $x \leq 0.55$ and $y \leq 0.175$ in the Al- and C-doped systems, respectively.

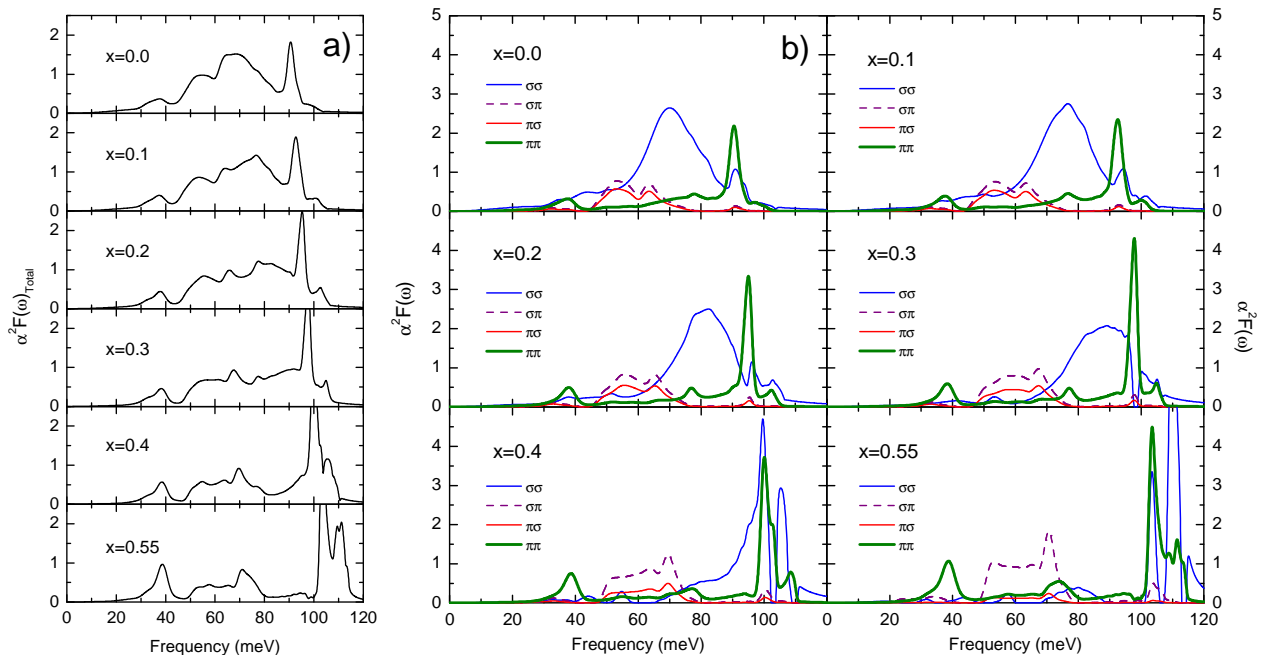


FIG. 1. (Color online) Evolution of the (a) total Eliashberg function and (b) components $\alpha_{ij}^2 F(\omega)$ ($i, j = \sigma, \pi$) for the Mg_{1-x}Al_xB₂ alloy.

In Fig. 1 we show the evolution of the Eliashberg functions, the total spectra and the four components $\alpha_{ij}^2 F(\omega)$ ($i, j = \sigma, \pi$) of Mg_{1-x}Al_xB₂ for six Al concentrations in the superconducting regime ($x = 0.0, 0.1, 0.2, 0.3, 0.4,$ and 0.55). We observe that for MgB₂ ($x = 0$) the largest contribution to the total spectral function comes from the $\sigma\sigma$ component, where the main peak centered at approximately 70 meV corresponds to frequency of the E_{2g} -phonon mode. The $\pi\pi$ spectrum has its main contribution from the high-frequency phonon region related to the B_{1g} -phonon mode, while the interband contribution, $\sigma\pi(\pi\sigma)$, is concentrated

in the region between 50 and 70 meV. We note that, although the $\sigma\sigma$ part represents the main contribution to the total spectra, the other components can not be neglected in a proper quantitative description of the e-ph coupling and of the superconducting properties.

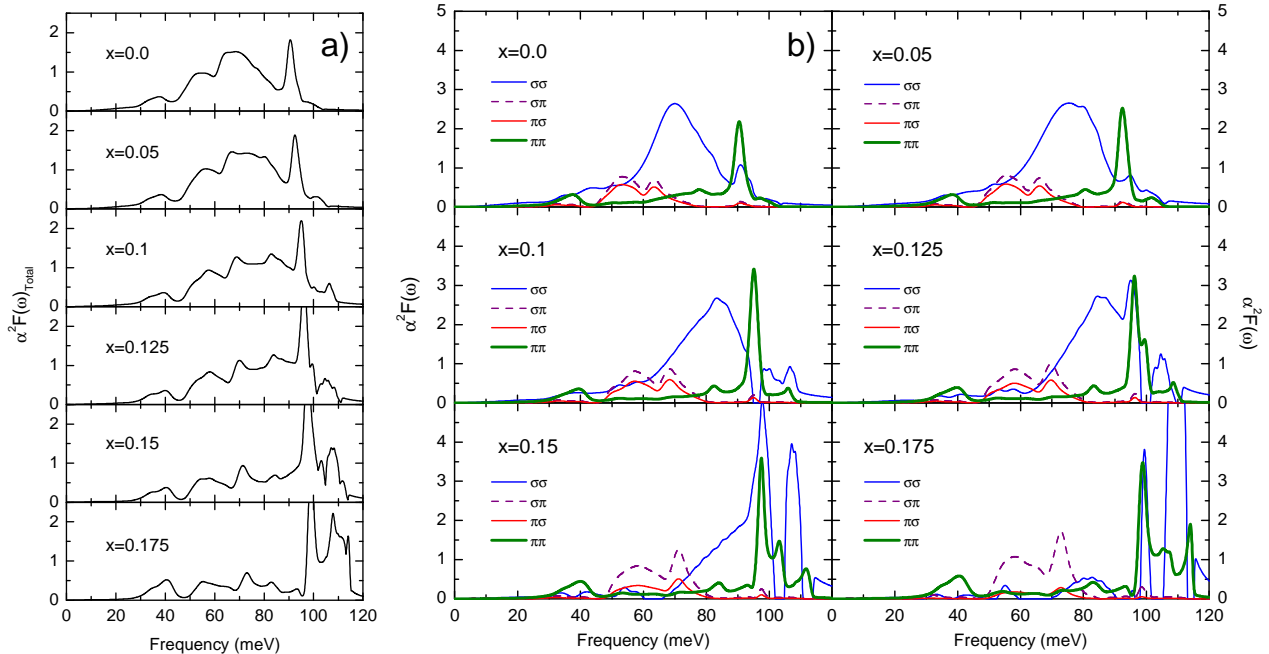


FIG. 2. (Color online) Evolution of the (a) total Eliashberg function and (b) components $\alpha_{ij}^2 F(\omega)$ ($i, j = \sigma, \pi$) for the MgB₂(1-y)C_{2y} alloy.

From the evolution of spectral functions for Mg_{1-x}Al_xB₂ (Fig. 1) we observe that almost all components are reduced by Al-doping, but the largest changes are exhibited by $\alpha_{\sigma\sigma}^2 F(\omega)$. Its main peak shifts to higher frequencies and its area is reduced at the same time until it practically vanishes for $x = 0.55$. This doping level is close to the region where the loss of superconductivity has been observed experimentally ($x \gtrsim 0.5$)¹⁸⁻²¹. The reduction of $\alpha_{\sigma\sigma}^2 F(\omega)$ indicates the loss of intraband e-ph coupling between the σ states and the bond-stretching phonon modes and has its origin in the continuous filling of the σ bands, which is completed at $x_c = 0.57$ ²⁸. The shift to higher frequencies is due to the hardening of the E_{2g} -phonon mode as x increases, a phenomenon discussed previously²⁸. Similar to $\sigma\sigma$, the $\pi\sigma$ interband contribution is also reduced as a function of x and almost disappears at $x = 0.55$. On contrast, the $\sigma\pi$ contribution shows a slight increase around 50 and 70 meV, and the $\pi\pi$ contribution at higher frequencies strengthens slightly with doping, but the position of

its main peak is almost unaffected. In recent electron tunneling spectroscopy measurements on Al-doped thin films³⁵, this general behavior of the Eliashberg function indeed has been observed, supporting our results.

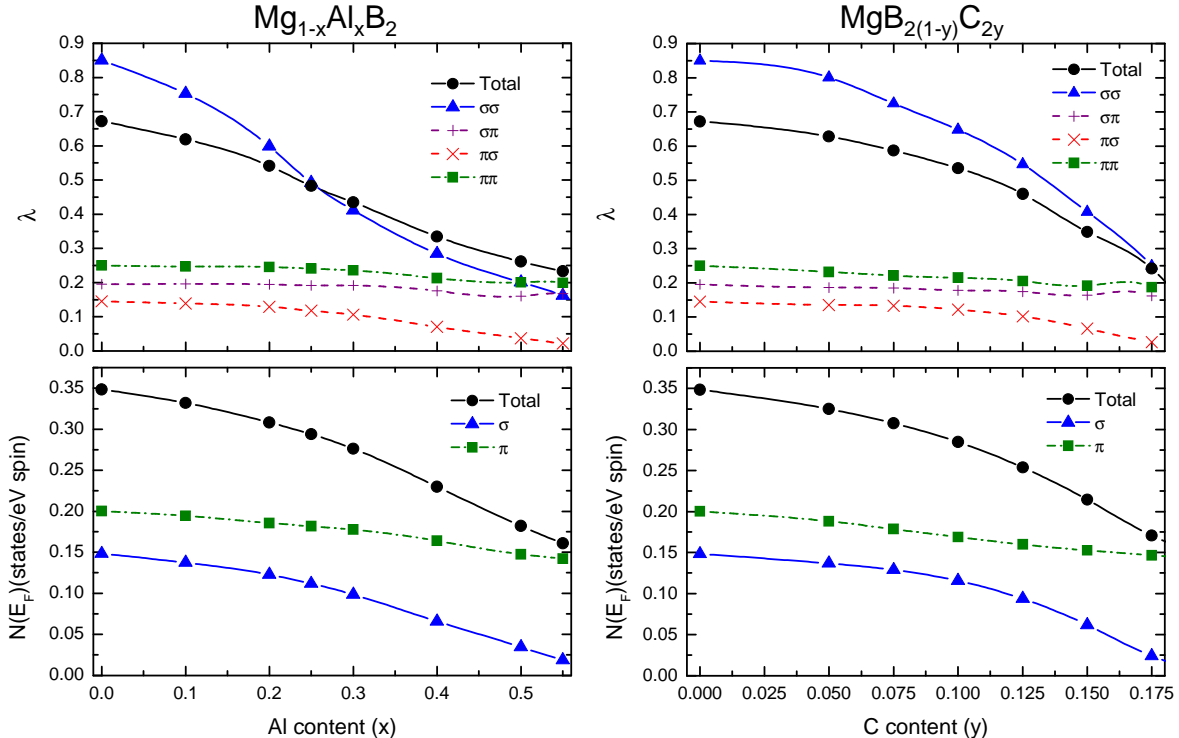


FIG. 3. (Color online) Evolution of λ_{ij} and $N_i(E_F)$ as a function of x and y for $\text{Mg}_{1-x}\text{Al}_x\text{B}_2$ and $\text{MgB}_{2(1-y)}\text{C}_{2y}$, respectively.

In Fig. 2 we present the results for the Eliashberg functions of $\text{MgB}_{2(1-y)}\text{C}_{2y}$ for six C concentrations in the superconducting region of the alloy ($y = 0.0, 0.05, 0.1, 0.125, 0.15,$ and 0.175). The different components of $\alpha^2F(\omega)$ exhibit the same trends with increasing C concentration as those found for the Al-doping. However the shape of the spectras are different and the changes take place at lower concentrations. When comparing the two alloys, one should take into account that the number of doping-induced electrons per unit cell is given by x and $2y$, respectively. Even with this factor of two, the vanishing of the $\sigma\sigma$ and $\sigma\pi$ contributions at $2y \approx 0.35$ occurs at a much smaller doping level than for Al-doping ($x = 0.55$). The dramatic reduction of $\alpha_{\sigma\sigma}^2F(\omega)$ at $y \approx 0.175$ correlates also with the complete filling of the σ -bands on $\text{MgB}_{2(1-y)}\text{C}_{2y}$ ²⁸.

In Fig. 3 calculated total and partial contributions for λ as well as for $N(E_F)$ are shown. For MgB_2 the calculated values are $\lambda_{\sigma\sigma} = 0.850$, $\lambda_{\sigma\pi} = 0.196$, $\lambda_{\pi\sigma} = 0.145$, $\lambda_{\pi\pi} = 0.250$, and

$\lambda_{tot} = 0.672$. It is worth mentioning that this λ_{tot} value is very close to the experimental one by Geerk *et al.*¹⁷ ($\lambda_{eff} = 0.650$). $N(E_F)$ partial contributions for MgB_2 are $N_\sigma = 0.148$ states $\text{eV}^{-1}/\text{spin}$ and $N_\pi = 0.200$ states $\text{eV}^{-1}/\text{spin}$, which are very similar to those calculated earlier by Liu *et al.*¹⁵ and Golubov *et al.*¹⁶. As seen from Fig. 3, the main contribution to the e-ph coupling (λ) in undoped MgB_2 comes from the $\sigma\sigma$ component. Among the different contributions of the e-ph coupling, $\lambda_{\sigma\sigma}$ shows the largest changes on doping with a reduction of $\approx 75\%$ (comparing the boundary concentrations). The other components also decrease with doping, albeit at different scales, ranging from the nearly constant behavior of $\lambda_{\sigma\pi}$ and $\lambda_{\pi\pi}$ to an almost complete vanishing of $\lambda_{\pi\sigma}$. As a consequence, λ_{tot} monotonically decreases with doping.

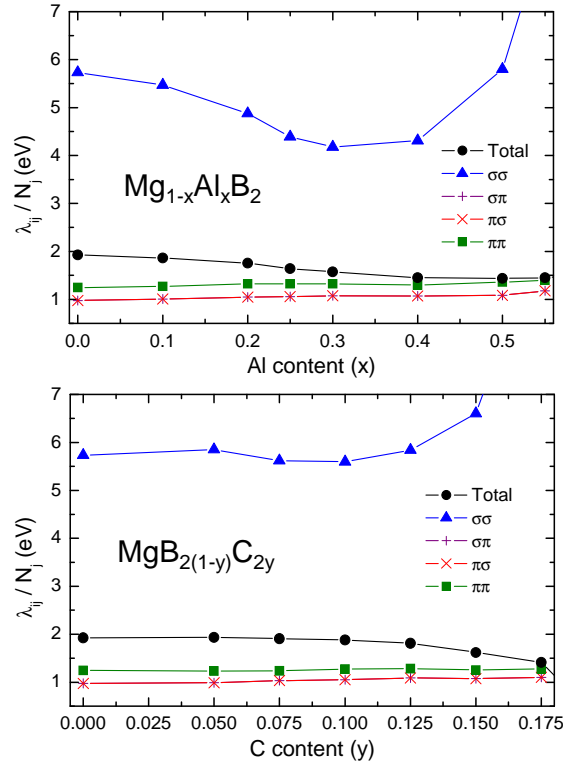


FIG. 4. (Color online) Evolution of λ_{ij}/N_j and λ_{tot}/N_{tot} as a function of x and y for $\text{Mg}_{1-x}\text{Al}_x\text{B}_2$ and $\text{MgB}_{2(1-y)}\text{C}_{2y}$, respectively. Note that $\lambda_{\pi\sigma}/N_\sigma \equiv \lambda_{\sigma\pi}/N_\pi$.

Doping-induced changes in the coupling constants can arise from changes in the partial density of states or from changes in the e-ph matrix elements. In order to distinguish between these two possibilities, we plotted in Fig. 4 the ratios λ_{ij}/N_j and λ_{tot}/N_{tot} . Indeed, a relationship $\alpha_{ij}^2 F(\omega) \sim N_j$ and $\lambda_{ij} \sim N_j$ can easily be derived from Eq. 1 under the

assumption of momentum-independent e-ph matrix elements. The ratios λ_{ij}/N_j for the interband ($\lambda_{\sigma\pi}$, $\lambda_{\pi\sigma}$) as well as for the intraband $\lambda_{\pi\pi}$ couplings remain practically constant as a function of doping for both alloys, indicating that the corresponding e-ph matrix elements are approximately independent of doping. However, for the ($\sigma\sigma$) intraband coupling, the ratio exhibits a stronger variation with doping, in particular for Al doping, which signals a clear doping dependence of the e-ph matrix elements. In this case, a simple scaling with the partial density of states would be inappropriate to describe the doping dependence of $\lambda_{\sigma\sigma}$.

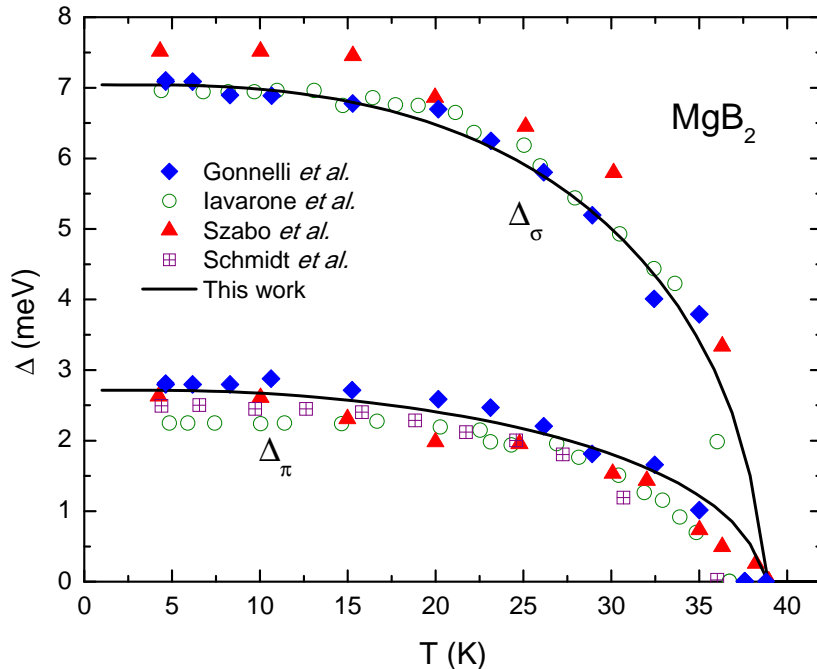


FIG. 5. (Color online) Temperature dependence of the superconducting gaps Δ_σ and Δ_π (solid lines) for undoped MgB_2 as obtained from the two-band Eliashberg gap equations. Symbols represent experimental data (\blacktriangle)⁷, (\circ)⁸, (\boxplus)⁹, and (\blacklozenge)^{10,34}. The calculated gap values at $T \rightarrow 0$ K are $\Delta_\sigma = 7.04$ meV and $\Delta_\pi = 2.71$ meV.

To solve the Eliashberg gap equations, we determined the single remaining parameter, the Coulomb pseudopotential μ_0^* , by the requirement that for undoped MgB_2 the experimental transition temperature of $T_c = 38.82\text{K}$ ^{31,34} is reproduced. For a cutoff frequency $\omega_c = 10\omega_{ph}^{max}$ we found $\mu_0^* = 0.107$. The resulting temperature dependence of the superconducting gaps is shown in Fig. 5 and compared with available experimental data^{7-9,34}. The gap values for $T \rightarrow 0$ K are $\Delta_\sigma = 7.04$ meV and $\Delta_\pi = 2.71$ meV, respectively, in good agreement with experimental results^{8,9,34}.

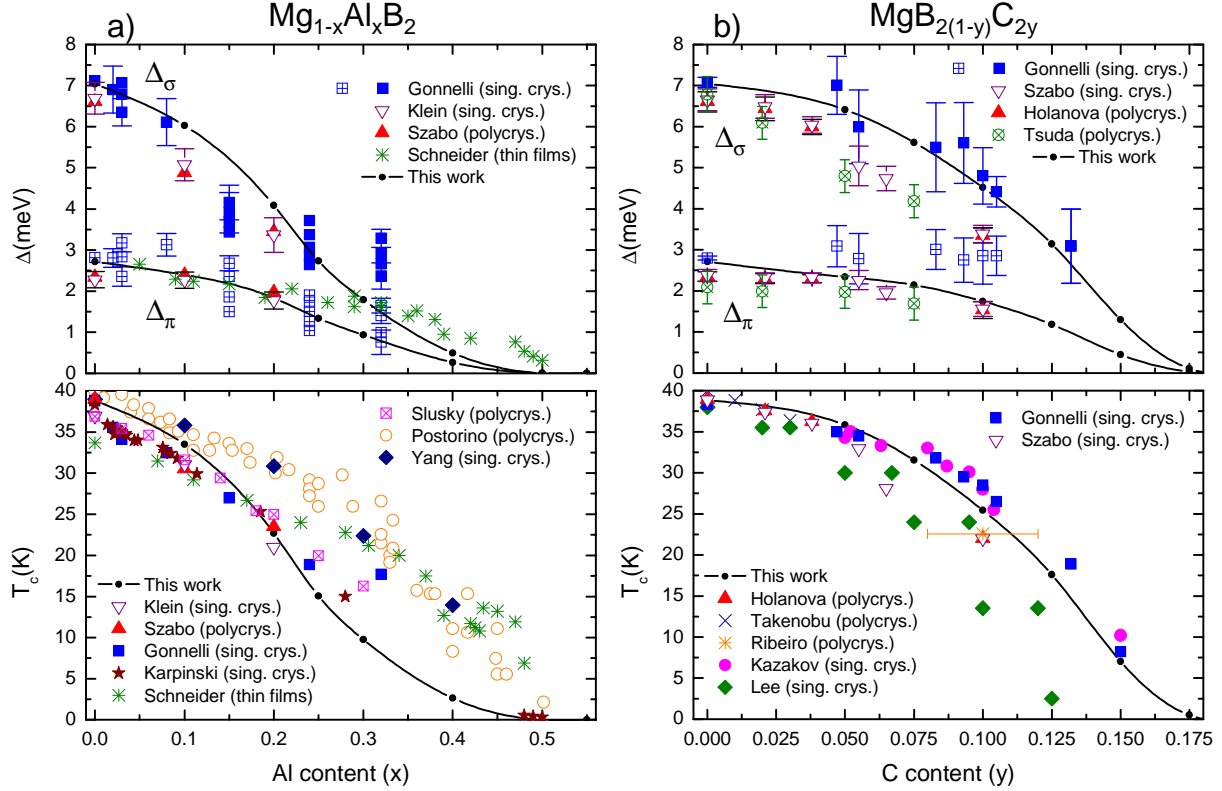


FIG. 6. (Color online) Superconducting gaps Δ_σ and Δ_π at $T \rightarrow 0\text{K}$ and critical temperature T_c for (a) $\text{Mg}_{1-x}\text{Al}_x\text{B}_2$ and (b) $\text{MgB}_{2(1-y)}\text{C}_{2y}$ as a function of x or y , respectively. The lines are the present calculations and the symbols represent various experimental measurements; (a): (\boxtimes)¹⁸, (\circ)²⁰, (\blacklozenge)²¹, (\blackstar)³⁰, (∇)³², (\blacktriangle)³³, (\boxplus , \blacksquare)^{31,34}, ($*$)³⁵; (b): (\times)²², ($*$)^{23,24}, (\bullet)²⁵, (\blacklozenge)²⁶, (∇)³³, (\boxplus , \blacksquare)^{31,34}, (\blacktriangle)³⁷, (\otimes)³⁸.

The same two-band Eliashberg approach was adopted for the alloys $\text{Mg}_{1-x}\text{Al}_x\text{B}_2$ and $\text{MgB}_{2(1-y)}\text{C}_{2y}$ keeping μ_0^* at the obtained value for undoped MgB_2 . The doping dependence of Δ_σ , Δ_π , and T_c for both alloys is presented in Fig. 6 and compared with experimental data^{18,20–26,30–35,37,38}. The calculations reproduce the experimental trends that both gaps and T_c decrease with increasing Al or C doping. Beside this common feature the two alloys exhibit also striking differences. The first concerns the doping range where superconductivity exists. T_c goes to zero close to the critical concentration for which the σ -band is completely filled ($x_c(\text{Al}) = 0.57$, $y_c(\text{C}) = 0.177$)²⁸. Thus, superconductivity vanishes significantly faster on C doping than on Al doping, even when taking into account that one should compare doping levels $x = 2y$ as discussed above. The second difference relates to the shape of the T_c versus doping curves. For Al doping, T_c initially drops fast and develops a longer tail,

whereas for C doping T_c is only slowly reduced initially, while it exhibits a steeper drop towards the critical concentration where T_c vanishes. A similar difference in shape is also observed for the larger gap. As both alloys are electron-doped systems, these differences indicate the importance of the doping site for the superconducting properties. As explained in Refs. 27 and 28, the origin of this difference can be traced back to the distribution of the extra charge introduced by doping. In the Al-doped system an important portion of the extra electrons is located in the interplanar region, and only a small fraction in the boron planes. In contrast, for C doping the extra charge mainly remains in the area between the B atoms within the boron plane, exactly in the region of the σ -bonds. Therefore, the extra charge introduced by C doping is more effective in reducing the number of holes in the σ -band and has a stronger influence on the phonon frequencies, in particular, on the hardening of the E_{2g} mode. Consequently, C doping leads to a faster decrease of the e-ph coupling and of the superconducting properties as compared to Al doping.

The various experimental data sets for T_c and the gaps plotted in Fig. 6 exhibit a clear spread indicating a large dependence of the superconducting properties on the sample preparation methods and on the physical conditions of the measurement procedure itself. In addition, an accurate determination of the actual doping concentration in these alloys is complicated and far from trivial. Furthermore, there is so far no consensus about the behavior of the gaps for larger C doping. While some experiments suggest a merging of the Δ_σ and Δ_π gap at $y \approx 0.13$ ^{31,34}, others find two distinct gaps even for the highest doping levels^{33,37,38}. Within these experimental uncertainties, our calculations agree quantitatively with the data for both alloys. In particular, the different doping regimes are obtained in a natural way. We recall that our study involved only a single free parameter, μ_0^* , which was fixed for the undoped system and which does not directly affect the doping dependence or the gap anisotropy.

In agreement with experimental data, the present calculation predicts for both alloys a stronger influence of doping on the σ gap, which follows approximately the doping dependence of T_c . On contrast, the π gap remains rather stable and only slowly decreases on doping. This is at variance with a previous *ab initio* study based on the fully anisotropic gap equations by Choi *et al.*⁴⁴, where doping was modeled by simply introducing excess electrons. For a moderate doping level of $x = 0.2$ ($y = 0.1$), they found a severe degradation of the π gap while the σ gap was more robust. This failure of a rigid-band-like type approach

indicates that a more self-consistent site-dependent treatment of the doping is required for a proper description of the superconducting properties in doped MgB₂.

Two previous computational studies^{51,52} of the superconducting properties of MgB₂ alloys adopted a scaling scheme to describe the doping dependence. The Eliashberg functions for the undoped compound were scaled taking into account the doping dependence of $N(E_F)$ and of the E_{2g} phonon frequency. As such an approach does not discriminate between the doping sites, Kortus *et al.*⁵² argued that the differences observed for Al and C doping are due to a larger interband scattering for C than for Al doping. The present study, however, demonstrates that the difference between Al and C doping appears naturally within the VCA approach, without the need to introduce another free parameter such as the interband scattering, as long as the influence of doping on the structure and on the lattice dynamics is properly taken into account.

IV. CONCLUSIONS

We have performed a *first-principles* study of the electron-phonon coupling and superconducting properties for the Mg_{1-x}Al_xB₂ and MgB_{2(1-y)}C_{2y} alloys as a function of x and y , respectively, by combining the self-consistent virtual-crystal approximation and the two-band Eliashberg model. For undoped MgB₂, the Eliashberg function possess a main peak at around 70 meV related to the E_{2g} -phonon mode coming from the $\sigma\sigma$ contribution, and a sharper peak at 90 meV which originates largely from the $\pi\pi$ contribution, and is related to the B_{1g} -phonon mode. The total coupling constant $\lambda_{tot} = 0.67$ agrees with the experimental value of 0.65 as deduced from tunneling measurements. For the alloys we found that $\alpha^2F(\omega)$ depends very sensitively on doping. It exhibits pronounced changes both in shape and in position of its main peaks, which renders any attempt to derive it from the spectrum of undoped MgB₂ via scaling procedures very unreliable. The calculated evolution of the Eliashberg functions compare well with recent electron tunneling spectroscopy measurements on Al-doped thin films. The e-ph coupling parameter and its different contributions decrease as a function of doping for both alloys. Although both Al and C dopants donate electrons, the e-ph coupling exhibits a clear dependence on the doping site, which is also reflected in $\alpha^2F(\omega)$. With the Coulomb pseudopotential fixed for the undoped compound, we could reproduce the experimental doping dependence of Δ_σ , Δ_π , and T_c for both alloys.

The observed differences between Al and C doping, like the doping range of superconductivity, are naturally obtained in the present VCA approach, without the need to invoke other factors, as, e.g., interband scattering. These results emphasize that a quantitative description of the superconducting properties of the two MgB₂ alloys require a proper treatment of the doping at least on the level of VCA, and suggest that interband scattering plays only a minor role.

ACKNOWLEDGMENTS

This research was supported by the Consejo Nacional de Ciencia y Tecnología (CONACYT, México) under Grant No. 43830-F and the Karlsruher Institut für Technologie (KIT), Germany. One of the authors (O.P.-S.) gratefully acknowledges CONACYT-México and the Deutscher Akademischer Austausch Dienst (DAAD).

-
- ¹ J. Nagamatsu, N. Nakagawa, T. Muranaka, Y. Zanitai, and J. Akimitsu, *Nature* **410**, 63 (2001).
 - ² J. M. An and W. E. Pickett, *Phys. Rev. Lett.* **86**, 4366 (2001).
 - ³ J. Kortus, I. I. Mazin, K. D. Belashchenko, V. P. Antropov, and L. L. Boyer, *Phys. Rev. Lett.* **86**, 4656 (2001).
 - ⁴ A. Q. R. Baron, H. Uchiyama, S. Tsutsui, Y. Tanaka, D. Ishikawa, J. P. Sutter, S. Lee, S. Tajima, R. Heid, and K. P. Bohnen, *Physica C* **456**, 83 (2007).
 - ⁵ A. Floris, A. Sanna, M. Lüders, G. Profeta, N. N. Lathiotakis, M. A. L. Marques, C. Franchini, E. K. U. Gross, A. Continenza, and S. Massidda, *Physica C* **546**, 45 (2007).
 - ⁶ J. Kortus, *Physica C* **546**, 54 (2007).
 - ⁷ P. Szabó, P. Samuely, J. Kačmarčík, T. Klein, J. Marcus, D. Fruchart, S. Miraglia, C. Marcenat, and A. G. M. Jansen, *Phys. Rev. Lett.* **87**, 137005 (2001).
 - ⁸ M. Iavarone, G. Karapetrov, A. E. Koshelev, W. K. Kwok, G. W. Crabtree, D. G. Hinks, W. N. Kang, E. M. Choi, H. J. Kim, H. J. Kim, and S. I. Lee, *Phys. Rev. Lett.* **89**, 187002 (2002).
 - ⁹ H. Schmidt, J. F. Zasadzinski, K. E. Gray, and D. G. Hinks, *Phys. Rev. Lett.* **88**, 127002 (2002).

- ¹⁰ R. S. Gonnelli, D. Daghero, G. A. Ummarino, V. A. Stepanov, J. Jun, S. M. Kazakov, and J. Karpinski, *Phys. Rev. Lett.* **89**, 247004 (2002).
- ¹¹ Y. Kong, O. V. Dolgov, O. Jepsen, and O. K. Andersen, *Phys. Rev. B* **64**, 020501 (2001).
- ¹² K. P. Bohnen, R. Heid, and B. Renker, *Phys. Rev. Lett.* **86**, 5771 (2001).
- ¹³ T. Yildirim, O. Gülseren, J. W. Lynn, C. M. Brown, T. J. Udovic, Q. Huang, N. Rogado, K. A. Regan, M. A. Hayward, J. S. Slusky, T. He, M. K. Haas, P. Khalifah, K. Inumaru, and R. J. Cava, *Phys. Rev. Lett.* **87**, 037001 (2001).
- ¹⁴ K. Kunc, I. Loa, K. Syassen, R. K. Kremer, and K. Ahn, *J. Phys.: Condens. Matter* **13**, 9945 (2001).
- ¹⁵ A. Y. Liu, I. I. Mazin, and J. Kortus, *Phys. Rev. Lett.* **87**, 087005 (2001).
- ¹⁶ A. A. Golubov, J. Kortus, O. V. Dolgov, O. Jepsen, Y. Kong, O. K. Andersen, B. J. Gibson, K. Ahn, and R. K. Kremer, *J. Phys.: Condens. Matter* **14**, 1353 (2002).
- ¹⁷ J. Geerk, R. Schneider, G. Linker, A. G. Zaitsev, R. Heid, K. P. Bohnen, and H. v. Löhneysen, *Phys. Rev. Lett.* **94**, 227005 (2005).
- ¹⁸ J. S. Slusky, N. Rogado, K. A. Regan, M. A. Hayward, P. Khalifah, T. He, K. Inumaru, S. M. Loureiro, M. K. Hass, H. W. Zandbergen, and R. J. Cava, *Nature* **410**, 343 (2001).
- ¹⁹ A. Bianconi, D. Di Castro, S. Agrestini, G. Campi, N. L. Saini, A. Saccone, S. De Negri, and M. Giovannini, *J. Phys.: Condens. Matter* **13**, 7383 (2001).
- ²⁰ P. Postorino, A. Congeduti, P. Dore, A. Nucara, A. Bianconi, D. Di Castro, S. De Negri, and A. Saccone, *Phys. Rev. B* **65**, 020507 (2001).
- ²¹ H. D. Yang, H. L. Liu, J. Y. Lin, M. X. Kuo, P. L. Ho, J. M. Chen, C. U. Jung, M. S. Park, and S. I. Lee, *Phys. Rev. B* **68**, 092505 (2003).
- ²² T. Takenobu, T. Ito, D. H. Chi, K. Prassides, and Y. Iwasa, *Phys. Rev. B* **64**, 134513 (2001).
- ²³ R. A. Ribeiro, S. L. Bud'ko, C. Petrovic, and P. C. Canfield, *Physica C* **384**, 227 (2003).
- ²⁴ M. Avdeev, J. D. Jorgensen, R. A. Ribeiro, S. L. Bud'ko, and P. C. Canfield, *Physica C* **387**, 301 (2003).
- ²⁵ S. M. Kazakov, J. Karpinski, J. Jun, P. Geiser, N. D. Zhigadlo, R. Puzniak, and A. V. Mironov, *Physica C* **408**, 123 (2004).
- ²⁶ S. Lee, T. Masui, A. Yamamoto, H. Uchiyama, and S. Tajima, *Physica C* **397**, 7 (2003).
- ²⁷ O. De la Peña, A. Aguayo, and R. de Coss, *Phys. Rev. B* **66**, 012511 (2002).

- ²⁸ O. De la Peña-Seaman, R. de Coss, R. Heid, and K. P. Bohnen, *Phys. Rev. B* **79**, 134523 (2009).
- ²⁹ R. S. Gonnelli, D. Daghero, A. Calzolari, G. A. Ummarino, V. Dellarocca, V. A. Stepanov, S. M. Kazakov, N. Zhigadlo, and J. Karpinski, *Phys. Rev. B* **71**, 060503 (2005).
- ³⁰ J. Karpinski, N. D. Zhigadlo, G. Schuck, S. M. Kazakov, B. Batlogg, K. Rogacki, R. Puzniak, J. Jun, E. Müller, P. Wägli, R. S. Gonnelli, D. Daghero, G. A. Ummarino, and V. A. Stepanov, *Phys. Rev. B* **71**, 174506 (2005).
- ³¹ R. S. Gonnelli, D. Daghero, G. A. Ummarino, M. Tortello, D. Delaude, V. A. Stepanov, and J. Karpinski, *Physica C* **456**, 134 (2007).
- ³² T. Klein, L. Lyard, J. Marcus, C. Marcenat, P. Szabó, Z. Hol'ánová, P. Samuely, B. W. Kang, H. J. Kim, H. S. Lee, H. K. Lee, and S. I. Lee, *Phys. Rev. B* **73**, 224528 (2006).
- ³³ P. Szabó, P. Samuely, Z. Pribulová, M. Angst, S. Bud'ko, P. C. Canfield, and J. Marcus, *Phys. Rev. B* **75**, 144507 (2007).
- ³⁴ D. Daghero, D. Delaude, A. Calzolari, M. Tortello, G. A. Ummarino, R. S. Gonnelli, V. A. Stepanov, N. D. Zhigadlo, S. Katrych, and J. Karpinski, *J. Phys.: Condens. Matter* **20**, 085225 (2008).
- ³⁵ R. Schneider, A. G. Zaitsev, O. De la Peña-Seaman, R. de Coss, R. Heid, K. P. Bohnen, and J. Geerk, *Phys. Rev. B* **81**, 054519 (2010).
- ³⁶ H. Schmidt, K. E. Gray, D. G. Hinks, J. F. Zasadzinski, M. Avdeev, J. D. Jorgensen, and J. C. Burley, *Phys. Rev. B* **68**, 060508(R) (2003).
- ³⁷ Z. Hol'ánová, P. Szabó, P. Samuely, R. H. T. Wilke, S. L. Bud'ko, and P. C. Canfield, *Phys. Rev. B* **70**, 064520 (2004).
- ³⁸ S. Tsuda, T. Yokoya, T. Kiss, T. Shimojima, S. Shin, T. Togashi, S. Watanabe, C. Zhang, C. T. Chen, S. Lee, H. Uchiyama, S. Tajima, N. Nakai, and K. Machida, *Phys. Rev. B* **72**, 064527 (2005).
- ³⁹ S. V. Barabash and D. Stroud, *Phys. Rev. B* **66**, 012509 (2002).
- ⁴⁰ S. Suzuki, S. Higai, and K. Nakao, *J. Phys. Soc. Japan* **70**, 1206 (2001).
- ⁴¹ P. P. Singh, *Solid State Commun.* **127**, 271 (2003).
- ⁴² D. Kasinathan, K. W. Lee, and W. E. Pickett, *Physica C* **424**, 116 (2005).
- ⁴³ L. D. Cooley, A. J. Zambano, A. R. Moodenbaugh, R. F. Klie, J. C. Zheng, and Y. Zhu, *Phys. Rev. Lett.* **95**, 267002 (2005).

- ⁴⁴ H. J. Choi, S. G. Louie, and M. L. Cohen, *Phys. Rev. B* **79**, 094518 (2009).
- ⁴⁵ B. Renker, K. P. Bohnen, R. Heid, D. Ernst, H. Schober, M. Koza, P. Adelman, P. Schweiss, and T. Wolf, *Phys. Rev. Lett.* **88**, 067001 (2002).
- ⁴⁶ G. Profeta, A. Continenza, and S. Massidda, *Phys. Rev. B* **68**, 144508 (2003).
- ⁴⁷ A. H. Moudden, *J. Phys. Chem. Solids* **88**, 067001 (2006).
- ⁴⁸ P. P. Singh, *Physica C* **382**, 381 (2002).
- ⁴⁹ A. Bussmann-Holder and A. Bianconi, *Phys. Rev. B* **67**, 132509 (2003).
- ⁵⁰ G. A. Ummarino, R. S. Gonnelli, S. Massidda, and A. Bianconi, *J. of Supercond.: Inc. Novel Magnetism* **18**, 791 (2005).
- ⁵¹ G. A. Ummarino, R. S. Gonnelli, S. Massidda, and A. Bianconi, *Physica C* **407**, 121 (2004).
- ⁵² J. Kortus, O. V. Dolgov, R. K. Kremer, and A. A. Golubov, *Phys. Rev. Lett.* **94**, 027002 (2005).
- ⁵³ P. J. T. Joseph and P. P. Singh, *Physica C* **454**, 43 (2007).
- ⁵⁴ J. W. Kohn and L. J. Sham, *Phys. Rev.* **140**, A1133 (1965).
- ⁵⁵ M. J. Mehl, D. Papaconstantopoulos, and D. J. Singh, *Phys. Rev. B* **64**, 140509 (2001).
- ⁵⁶ O. De la Peña-Seaman, R. de Coss, R. Heid, and K. P. Bohnen, *Phys. Rev. B* **76**, 174205 (2007).
- ⁵⁷ O. De la Peña-Seaman, R. de Coss, R. Heid, and K. P. Bohnen, *J. Phys.: Condens. Matter* **19**, 476216 (2007).
- ⁵⁸ S. G. Louie, K. M. Ho, and M. L. Cohen, *Phys. Rev. B* **19**, 1774 (1979).
- ⁵⁹ B. Meyer, C. Elsässer, and M. Fähnle, FORTRAN90 Program for Mixed-Basis Pseudopotential Calculations for Crystals, Max-Planck-Institut für Metallforschung, Stuttgart (unpublished).
- ⁶⁰ D. Vanderbilt, *Phys. Rev. B* **32**, 8412 (1985).
- ⁶¹ D. A. Papaconstantopoulos, E. N. Economou, B. M. Klein, and L. L. Boyer, *Phys. Rev. B* **20**, 177 (1979).
- ⁶² C. Ambrosch-Draxl, P. Süle, H. Auer, and E. Y. Sherman, *Phys. Rev. B* **67**, 100505 (2003).
- ⁶³ T. Thonhauser and C. Ambrosch-Draxl, *Phys. Rev. B* **67**, 134508 (2003).
- ⁶⁴ S. Baroni, P. Giannozzi, and A. Testa, *Phys. Rev. Lett.* **58**, 1861 (1987).
- ⁶⁵ P. Giannozzi, S. de Gironcoli, P. Pavone, and S. Baroni, *Phys. Rev. B* **43**, 7231 (1991).
- ⁶⁶ R. Heid and K. P. Bohnen, *Phys. Rev. B* **60**, R3709 (1999).
- ⁶⁷ G. M. Eliashberg, *Sov. Phys. JETP* **11**, 696 (1960).

- ⁶⁸ J. P. Carbotte, *Rev. Mod. Phys.* **62**, 1027 (1990).
- ⁶⁹ F. Marsiglio and J. P. Carbotte, *The Physics of Superconductors*, Vol. I. Conventional and High- T_c Superconductors (Springer-Verlag Berlin, Heidelberg, 2003) pp 231.
- ⁷⁰ S. Y. Savrasov, D. Y. Savrasov, and O. K. Andersen, *Phys. Rev. Lett.* **72**, 372 (1994).
- ⁷¹ V. Ozolins and M. Korling, *Phys. Rev. B* **48**, 18304 (1993).
- ⁷² J. P. Perdew, K. Burke, and M. Ernzerhof, *Phys. Rev. Lett.* **77**, 3865 (1996).
- ⁷³ K. Kokko and M. P. Das, *J. Phys.: Condens. Matter* **10**, 1285 (1998).
- ⁷⁴ V. Z. Kresin and S. A. Wolf, *Phys. Rev. B* **46**, 6458 (1992).
- ⁷⁵ I. I. Mazin, O. K. Andersen, O. Jepsen, A. A. Golubov, O. V. Dolgov, and J. Kortus, *Phys. Rev. B* **69**, 056501 (2004).
- ⁷⁶ In some previous works (Refs. 77–79) also an uniform matrix form for the Coulomb pseudopotential matrix has been adopted. It has been demonstrated that this specific form underestimates considerably the value of Δ_π (Ref. 75). However, we tested another form used in previous publications (Refs. 16 and 51) where the diagonal elements are considered to be different between them additionally off-diagonal ones are included, nevertheless they are much smaller than the diagonal ones. Results in Section III were practically the same for both forms, except for a slight reduction of Δ_π by 10%.
- ⁷⁷ H. J. Choi, D. Roundy, H. Sun, M. L. Cohen, and S. G. Louie, *Nature* **418**, 758 (2002).
- ⁷⁸ H. J. Choi, D. Roundy, H. Sun, M. L. Cohen, and S. G. Louie, *Phys. Rev. B* **66**, 020513 (2002).
- ⁷⁹ H. J. Choi, D. Roundy, H. Sun, M. L. Cohen, and S. G. Louie, *Phys. Rev. B* **69**, 056502 (2004).